PAPER

Check for updates

Carotane sesquiterpenes from *Ferula vesceritensis*: *in silico* analysis as SARS-CoV-2 binding inhibitors†

Tarik A. Mohamed,[a] Abdelsamed I. Elshamy,[b] Mahmoud A. A. Ibrahim, [iD][c]
Ammar Zellagui,[d] Mahmoud F. Moustafa,[ef] Alaa H. M. Abdelrahman,[c] Shinji Ohta,[g]
Paul W. Pare [iD] *[h] and Mohamed-Elamir F. Hegazy*[a]

Two sesquiterpenes, 8α-anisate-dauc-4-ene-3,9-dione (webiol anisate) (**1**) and 10α-acetoxy-6α-benzoate-jaeschkeanadiol (**2**) as well as, ten known analogues (**3–10**), and two sesquiterpene coumarins (**11–12**) were isolated from an organic root extract of *Ferula vesceritensis* (Fam. Apiaceae). Chemical structures were elucidated based on IR, 1D- and 2D-NMR and HRMS, spectroscopic analyses. With molecular overlap observed between two protease inhibitors that are being examined as anti-COVID-19 drugs, and sesquiterpenes isolated here, metabolite molecular docking calculations were made using the main protease (M^{pro}), which is required for viral multiplication as well as RNA-dependent RNA polymerase (RdRp). *In silico* binding-inhibition analysis predicted that select *F. vesceritensis* sesquiterpenes can bind to these enzymes required for viral replication. Structures of the isolated constituents were also consistent with the chemo-systematic grouping of *F. vesceritensis* secondary metabolites with other *Ferula* species.

Introduction

The genus *Ferula*, composed of approximately 180 species, is the third-largest genus in the Apiaceae family. Over 130 species are distributed throughout the Mediterranean and Central Asia region.[1,2] Many *Ferula* species are used as traditional medicines for treatments such as impotency and frigidity, skin infections, dysentery, neurological disorders (tranquillizer, anti-hysteric), rheumatism, headache, digestive disorders, dizziness and arthritis.[3–5] Resins of *Ferula* are used as a febrifuge as well as a carminative agent for stomach disorders.[1] Some *Ferula* species

exhibit anticancer,[6,7] anthelmintic,[7] antimicrobial,[6,8] anti-fungal,[7] anticonvulsant,[9] antioxidant,[6,10] antiproliferative,[11,12] anti-hypertensive,[13] hepatoprotective[7] and antibiotic-odulation[6] agents. Previous phytochemical studies of *Ferula* species revealed that the main constituents are sesquiterpenes.[14]

Ferula vesceritensis (Batt.), also known as *F. tingitana* L. var, is endemic to Algeria and Libya, where it is used as traditional medicine for the treatment of inflammatory, cancer, fever, headaches and throat infections; livestock are observed to avoid grazing on the foliage.[15] Previous *F. vesceritensis* phytochemical studies report the accumulation of sesquiterpenes and sesqui-terpene coumarins.[15,16] With the recent COVID-19 pandemic, the question arises as to whether secondary metabolites from *F. vesceritensis* can serve as inhibitors of enzymes that participate in viral replication.

From the outset, COVID-19 was identified as a new beta coronavirus, initially referred to as SARS-CoV-2 and later named coronavirus disease-2019 (COVID-19) by the World Health Organization.[17] Infections are rapidly spread by respiratory droplets with a high mortality rate in select countries; the pandemic is a significant challenge to public health. With currently no specific antiviral drugs or vaccines developed to treat COVID-19, the virus is more deadly than the SARS, H1N1, MERS, and Ebola epidemics combined with more than 200 000 lives lost to the disease in the first half of 2020. Very recently, the U.S. Food and Drug Administration (FDA) has issued an emergency use authorization of remdesivir for treatment of suspected or laboratory-confirmed COVID-19 cases.

[a]Chemistry of Medicinal Plants Department, National Research Centre, 33 El-Bohouth St., Dokki, Giza, 12622, Egypt. E-mail: me.fathy@nrc.sci.eg; Fax: +20-23337093

[b]Chemistry of Natural Compounds Department, National Research Centre, 33 El Bohouth St., Dokki, Giza, 12622, Egypt

[c]Computational Chemistry Laboratory, Chemistry Department, Faculty of Science, Minia University, Minia 61519, Egypt

[d]Laboratory of Biomolecule and Plant Breeding, Life Science and Nature Department, Faculty of Exact Science and Life Science and Nature, University of Larbi Ben Mhidi, 4000 Oum El Bouaghi, Algeria

[e]Department of Biology, College of Science, King Khalid University, 9004, Abha, Kingdom of Saudi Arabia

[f]Department of Botany & Microbiology, Faculty of Science, South Valley University, Qena, Egypt

[g]Graduate School of Integrated Sciences for Life, Hiroshima University, 1-7-1 Kagamiyama, Higashi-Hiroshima 739-8521, Japan

[h]Department of Chemistry and Biochemistry, Texas Tech University, Lubbock, TX 79409, USA. E-mail: paul.pare@ttu.edu; Fax: +1 806 742 1289

† Electronic supplementary information (ESI) available. See DOI: 10.1039/d0ra06901a

In seeking chemical inhibitors to block COVID-19 replication, the molecular docking technique was utilized to predict binding affinities for compounds isolated from *F. vesceritensis* against SARS-CoV-2 main protease (M^{pro}) and RNA-dependent RNA polymerase (RdRp), two essential enzymatic components required for viral replication. Compounds included two new sesquiterpenes (**1,2**) in addition to ten previously reported compounds (**3–12**) (Fig. 1). Chemo-systematic significance of metabolites from *F. vesceritensis* was also compared with other members of the *Ferula* genus.

Results and discussion

Extensive fractionation and purification of the organic extract of *F. vesceritensis* afforded two new sesquiterpene, 8β-anisate-dauc-4-ene-3,9-dione (webiol anisate) (**1**) and 10β-acetoxy-6α-benzoate-jaeschkeanadiol (**2**) as well as ten previously reported compounds, 10α-acetoxy-6α-anisate-jaeschkeanadiol (**3**),[18] 2α-acetoxy-10β-hydroxy-6α-anisate-jaeschkeanadiol (**4**),[18] 2-oxoferutidin (**5**),[19] 2α-acetoxy-6α-*p*-methoxybenzoyl-10α-acetoxy-jaeschkeanadiol (**6**),[18] 2α-acetoxy-6α-*p*-methoxybenzoyl-10β-acetoxy-jaeschkeanadiol (**7**),[18] 2-acetoxy-6-*p*-methoxybenzoyl-jaeschkeanadiol (**8**),[20] 2α-hydroxy-6α*p*-methoxybenzoyl-10β-acetoxy-jaeschkeanadiol (**9**),[21] epoxyvesceritenol (**10**),[15] coladonin (**11**),[22] feselol (**12**).[16,23] Structures for the known metabolites were elucidated by comparison of collected spectroscopic data (1D- and 2D-NMR as well as MS data) with literature reports.

Compound **1** was obtained as a reddish amorphous powder with an optical rotation of ([α]$_D^{25}$ +56.9) in MeOH. TOF-ESI-MS analysis showed molecular ion peak at *m/z* 407.1827 [M + Na]$^+$ (calcd for $C_{23}H_{28}NaO_5^+$, 407.1834) indicating a molecular formula of $C_{23}H_{28}O_5$. The ^{13}C NMR spectrum displayed 23 carbon signals that categorized to 9 quaternary carbons

(comprising two keto groups at δ_C 205.8, 206.4), 5 methines, 4 methylenes, 5 methyls (including one methyl of methoxy). From all characterized carbons, *para*-anisate moiety (δ_C 166.3, 121.9, 132.2, 114.3 and 164.3), were clearly assigned. ^1H NMR data revealed the presence of an isopropyl moiety signals at δ_H 1.20 (3H, d, *J* = 7.0 Hz), 1.22 (3H, d, *J* = 7.0 Hz) and 2.65 (1H, m)]. In addition to methyl groups at δ_H 1.04 (3H, s) and 1.69 (3H, s), an anisate moiety with characteristic aromatic protons at δ_H 8.24 (2H, d, *J* = 8.9 Hz), 7.07 (2H, d, *J* = 8.9 Hz) and methoxy protons at δ_H 3.72 (s) were observed. These structural elements suggested a carotane skeleton corresponding to a bicyclic structure with a condensed seven and five membered ring system, as previously isolated from several *Ferula* species.[15,16,19,24,25] $^1H–^1H$ COSY indicated a blocked correlation between methine proton at δ_H 2.65 (m) and two methyl signals at δ_H 1.20 (3H, d, *J* = 7.0 Hz), δ_H 1.22 (3H, d, *J* = 7.0 Hz), indicating that the isopropyl group was located on quaternary olefinic carbon δ_C 143.9. Additionally, a characteristic methyl signal at δ_H 1.04 (s) for H-15 showed an HMBC correlation with olefinic quaternary carbon at δ_C 175.2 as well as methine proton at δ_H 2.65 (m). Accordingly, isopropyl signals at δ_H 1.20d (*J* = 7.0 MHz), 1.22d (*J* = 7.0 MHz) and 2.65 m were assigned H-12, H-13, and H-11, respectively. The quaternary olefinic carbons at δ_C 143.9 and 175.2 were assigned to C-4 and C-5, respectively. The methine proton, H-11, showed HMBC correlations with two olefinic quaternary carbon at 143.9 (C-4), 175.2 (C-5), a keto group at δ_C 206.4 was assigned to C-3. H-15 showed HMBC correlations with quaternary aliphatic carbon at δ_C 41.1 and two aliphatic methylene carbons at δ_C 48.9, 43.0 assigned to C-1, C-2, and C-10 respectively that associated with the cyclopentane ring. The remaining proton signals for two methylene groups with a vicinal relationship was deduced *via* COSY and HSQC analyses [δ_H 2.74 (1H, m), 2.83 (1H, m) and δ_C 21.1] and [δ_H 1.53 (1H, m), 2.65 (1H, m) and δ_C 40.7] and HMBC analysis confirm localization to C-6 and C-7. Finally, the location of the anisate moiety was deduced by the correlation between the proton at δ_H 1.69 s (H-14) and C-7 (δ_C 40.7), keto group at δ_C 205.8 and a quaternary carbon with an oxygen function (δ_C 86.0) indicating that the anisate group and CH$_3$-14 attached to a quaternary carbon with an oxygen function δ_C 86.0 (C-8). These correlations also confirmed the presence of the ketone at C-9. The position of the anisate at C-8 was as well deduced from the comparison of the NMR spectra with those the anisate derivative of webdiol that characterized by presence of a cycloheptane ring at C-8.[15,19,25] The relative stereochemistry was deduced through coupling constants and NOESY analysis. NOESY correlations of H-15 with H-2β and H-10β, and H-10β with H-14 showed that H-15, H-14 are in a β orientation. Thus, the structure of **1** was determined as 8α-anisate-dauc-4-ene-3,9-dione.

Compound **2** was obtained as a reddish amorphous powder with an optical rotation of ([α] +20) in MeOH. TOF-ESI-MS analysis showed a molecular ion peak at *m/z* 400.2249 [M]$^+$ (calcd for $C_{24}H_{32}O_5^+$, 400.2222) indicating a molecular formula of $C_{24}H_{32}O_5$. ^1H NMR data revealed the presence of an isopropyl moiety with signals at δ_H 0.83 (3H, d, *J* = 6.6 Hz), 0.96 (3H, d, *J* = 6.6 Hz) and 1.95 (1H, m)]. In addition to methyl groups at δ_H 1.18 (3H, s), 1.82 (3H, s) and 2.07 (3H, s); a benzoate moiety with
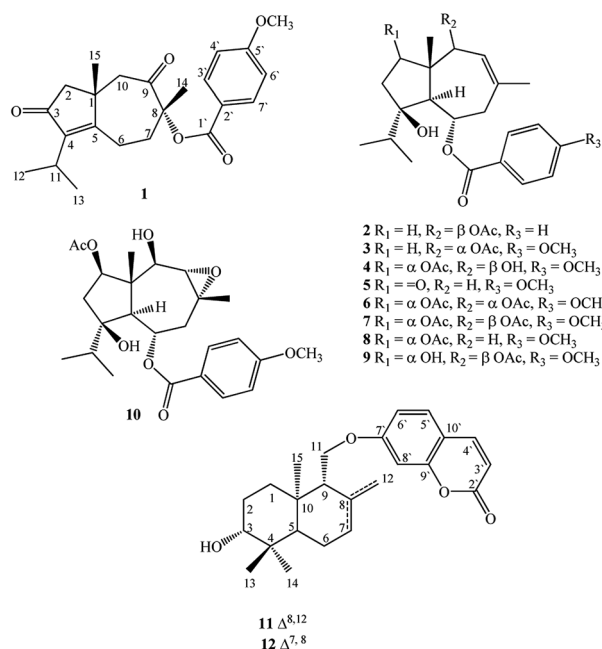
Fig. 1 Isolated compounds from *Ferula vesceritensis*.

2 R_1 = H, R_2 = β OAc, R_3 = H
3 R_1 = H, R_2 = α OAc, R_3 = OCH$_3$
4 R_1 = α OAc, R_2 = β OH, R_3 = OCH$_3$
5 R_1 = =O, R_2 = H, R_3 = OCH$_3$
6 R_1 = α OAc, R_2 = α OAc, R_3 = OCH$_3$
7 R_1 = α OAc, R_2 = β OAc, R_3 = OCH$_3$
8 R_1 = α OAc, R_2 = H, R_3 = OCH$_3$
9 R_1 = α OH, R_2 = β OAc, R_3 = OCH$_3$

11 Δ^{8,12}
12 Δ^{7,8}

characteristic aromatic protons at δ_H 8.00 (2H, d, $J = 7.2$ Hz), 7.46 (2H, t, $J = 7.8$ Hz) and 7.58 (1H, t, $J = 7.8$ Hz) was observed. The ^{13}C NMR spectrum displayed 24 carbon signals (Table 1), which were further differentiated by DEPT to 5 methyls (1 acetate group), 3 methylenes, 10 methines (two oxygenated, 6 olefinic) and 5 quaternary carbons (1 oxygenated, 2 keto, 2 olefinic). Spectroscopic data were similar to **3** except the appearance of an additional olefinic proton at δ_H 7.58 (1H, t, $J = 7.8$) and the disappearance of methoxy protons. This methoxy substitution was confirmed by ^{13}C-NMR analysis. 2D NMR (COSY, HMQC and HMBC) analyses (Fig. 2) and comparisons with published analogues indicated a 7/5 bicyclic cadinane-type sesquiterpene previously isolated from different *Ferula* species.[15,16,19,24,25] The two methylene groups with a vicinal attached to the methine carbon δ_C 70.4 (C-6) and that the carbons signals at δ_C 41, 130.2 and 128.8 are assigned to C-7, C-8 and C-9, respectively. These data confirm the presence of an acetate group at C-10 attached to the methine carbon δ_C 70.4 (C-6) and that the carbons signals at δ_C 41, 130.2 and 128.8 are assigned to C-7, C-8 and C-9, respectively. These data confirm the presence of an acetate group at C-10. The two methylene groups with a vicinal relationship deduced *via* COSY and HSQC analysis [δ_H 1.68 (m), 1.24 (m) and δ_C 37.5] and [H-3 at δ_H 1.57 m, 1.93 m and δ_C 31.2] and a blocked correlation between methine proton at δ_H 1.95 (m) and two methyl signals at δ_H 0.83 (3H, d, $J = 6.6$ Hz), δ_H 0.96 (3H, $J = 6.6$ Hz) were observed. Long-range ^{1}H–^{13}C correlations associated with two methyl groups (δ_H 0.83 and 0.96) to the carbon signals at δ_C 37.3 and 86.5 as well as methylene protons H-2 δ_H 1.68 (m), 1.24 (m) and H-3 at δ_H 1.57 m, 1.93 m were also observed. Additionally,
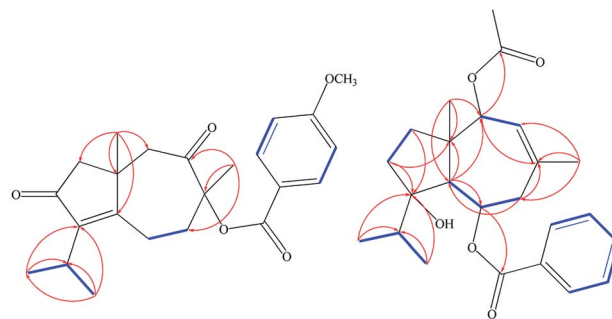

Fig. 2 Selected ^{1}H–^{1}H COSY (—) and HMBC (→) correlations of **1,2**.

a characteristic methyl signal at δ_H 1.20 s for H-15 showed correlation with the carbon signals at δ_C 48.2 (C-1), 37.7 (C-2), 57.7 (C-5) and 80.7 (C-10) indicating that the isopropyl group and acetate groups were located on quaternary oxygenated carbon δ_C 86.5 for C-4 and oxygenated methine carbon at δ_C 80.7 for C-10 respectively. Finally, the location of the benzoate moiety was deduced by the correlation between the olefinic methyl at δ_H 1.82 s for H-14 *via* HMBC correlations with carbons signals at δ_C 130.2, 128.8 and the carbon of methylene at δ_C 41.2 as well as H-5 at δ_H 2.11 d (10.8). In addition, correlations of H-5 with carbon of oxygenated methine at δ_C 70.4 were observed; these correlations indicate that the benzoate group is attached to the methine carbon δ_C 70.4 (C-6) and that the carbons signals at δ_C 41, 130.2 and 128.8 are assigned to C-7, C-8 and C-9, respectively. These data confirm the presence of an acetate group at C-10.

Table 1 ^{1}H (500 MHz) and ^{13}C (125 MHz) NMR chemical shifts for **1** and **2**

	1		**2**	
	^{1}H NMR (C$_5$D$_5$N, J MHz)	^{13}C NMR (C$_5$D$_5$N)	^{1}H NMR (CDCl$_3$, J MHz)	^{13}C NMR (CDCl$_3$)
1	—	41.1	—	48.2
2	2.24 br d (17.4), 3.00 br d (17.4)	48.9	1.68 m, 1.24 m	37.5
3	—	206.4	1.57 m, 1.93 m	31.2
4	—	143.9	—	86.5
5	—	175.2	2.11 d (10.8)	57.7
6	2.74 m, 2.83 m	21.1	5.30 td (10.8, 3.0)	70.4
7	1.53 m, 2.65 m	40.7	2.53 t (12.0), 2.30 dd (14.4, 3.0)	41.2
8	—	86.0	—	130.2
9	—	205.8	5.25 br s	128.8
10	2.44 d (12.4), 3.11 d (12.4)	43.0	5.22 br s	80.7
11	2.65 m	25.5	1.95 m	37.3
12	1.20 d (7.0)	20.2	0.83 d (6.6)	17.4
13	1.22 d (7.0)	20.3	0.96 d (6.6)	18.5
14	1.69 s	21.4	1.82 s	26.4
15	1.04 s	29.3	1.18 s	15.7
1′	—	166.3	—	166.4
2′	—	121.9	—	131.5
3′,7′	8.24 d (8.9)	132.2	8.00 d (7.2)	129.6
4′,6′	7.07 d (8.9)	114.3	7.46 t (7.8)	128.6
5′	—	164.3	7.58 t (7.8)	133.3
OCH$_3$	3.72 s	55.4	—	—
C=O, OAc	—	—	—	170.8
CH$_3$, OAc	—	—	2.07 s	21.2

The relative stereochemistry was deduced *via* a coupling constant, a td for proton at δ_H 5.30 (1H, J = 10.8, 3.0, H-6) is characteristic for the C-6β geminal proton of trans-fused daucane skeletons.[18] A small coupling between protons at δ_H 5.25 (1H, s, H-9) and 5.22 (1H, s, H-10) was only possible when the proton at C-10 in α orientation; therefore acylated group at C-10 in the β orientation.[18,21] The structure of **2** was therefore identified as 10β-acetoxy-6α-benzoate-jaeschkeanadiol.

Molecular docking

Utilizing AutoDock molecular docking software, binding affinities were predicted for isolated compounds **1–12** with SARS-CoV-2 M[pro] and RdRp to inhibit SARS-CoV-2 replication. The predicted binding affinities are listed in Table 2 and compared to two human immunodeficiency virus (HIV) protease inhibitors that have recently been subjected to clinical investigations as promising anti-COVID-19 drugs:[26] darunavir (DrugBank code: DB01264) and lopinavir (DrugBank code: DB01601). Two-dimensional representations for binding modes of **1–12** as well as darunavir and lopinavir inside the active sites of SARS-CoV-2 M[pro] and RdRp are depicted in Fig. S2 and S3,† respectively. The assayed natural products exhibited intermediate binding affinities towards SARS-CoV-2 M[pro], and RdRp with docking scores ranged from −9.9 to −6.7 and from −7.6 to −6.4 kcal mol⁻¹, respectively (Table 2). The observed high affinities are attributed to multiple hydrogen bonds, van der Waals and hydrophobic interactions between the natural products and proximal amino acids in the enzyme active site for M[pro] and RdRp. Compound **1** demonstrated the highest binding affinities of −9.9 and −7.6 kcal mol⁻¹, forming three hydrogen bonds with HIS163 (1.81 Å) and GLU166 (2.10, 2.08 Å), and six hydrogen bonds with TYR619 (1.99 Å), LYS621 (1.84, 2.05, 2.39 Å), CYS622 (1.78 Å) and LYS798 (2.21 Å) inside the active sites of M[pro] and RdRp, respectively (Fig. 3 and 4).

Table 2 Calculated docking scores (in kcal mol⁻¹) and binding features for the identified compounds **1–12** with SARS-CoV-2 main protease (M[pro]) and RNA-dependent RNA polymerase (RdRp)

Compound	Main protease (M[pro])		RNA-dependent RNA polymerase (RdRp)	
	Docking score (kcal mol⁻¹)	Binding features (hydrogen bond length in Å)	Docking score (kcal mol⁻¹)	Binding features (hydrogen bond length in Å)
1	−9.9	HIS163 (1.81 Å), GLU166 (2.10, 2.08 Å)	−7.7	TYR619 (1.99 Å), LYS621 (1.84, 2.05, 2.39 Å), CYS622 (1.78 Å), LYS798 (2.21 Å)
2	−8.8	GLY143 (1.95 Å), GLU166 (2.06 Å)	−7.5	LYS621 (1.96, 2.11 Å)
3	−6.6	—	−6.9	ASP618 (2.23 Å), ASP623 (2.86 Å), CYS622 (2.02 Å), TRP800 (1.96 Å)
4	−7.4	GLU166 (2.45 Å)	−6.2	TRP619 (2.21, 2.05 Å), CYS622 (2.10 Å)
5	−8.8	GLY143 (2.08 Å), CYS145 (2.67 Å), GLU166 (2.27 Å)	−6.4	ASP618 (2.19 Å), TRP800 (1.96 Å), LYS621 (2.77 Å)
6	−8.5	HIS163 (2.12 Å), GLU166 (2.70 Å), THR190 (2.41 Å), GLN192 (1.79, 2.20 Å)	−6.4	ASP618 (2.29 Å), LYS621 (2.09 Å), TRP800 (1.96 Å)
7	−8.0	GLU166 (2.24 Å), GLN192 (2.00 Å)	−7.1	ASP618 (2.26 Å), LYS621 (2.25, 2.52 Å), TRP800 (2.14 Å)
8	−9.0	GLY143 (2.47 Å), CYS145 (1.87, 2.67 Å), THR190 (2.89 Å)	−6.4	ASP618 (2.22 Å), LYS621 (2.20 Å), TRP800 (2.07 Å)
9	−6.4	—	−6.5	ASP618 (2.33 Å), ASP623 (2.95 Å), CYS622 (1.90 Å), TRP800 (2.02 Å)
10	−9.7	CYS145 (1.86 Å), GLU166 (2.61 Å), GLN189 (2.80 Å), THR190 (2.75 Å)	−6.9	LYS621 (1.98 Å), ASP760 (1.81 Å), TRP800 (1.81 Å)
11	−8.0	GLU166 (2.20 Å)	−6.4	TYR619 (2.34 Å), LYS621 (2.74 Å), GLU811 (1.88 Å)
12	−8.1	MET49 (3.04 Å), SER144 (2.21 Å), GLN189 (2.92 Å)	−6.6	ASP623 (2.11 Å), GLU811 (1.74 Å)
Darunavir	−8.2	GLU166 (1.94, 2.88 Å), LEU167 (1.96 Å)	−4.4	TYR619 (2.11 Å), ASP760 (1.83 Å), GLU811 (2.24, 2.26 Å)
Lopinavir	−9.8	LEU141 (1.96 Å), GLY143 (2.01 Å), SER144 (3.09 Å), HIS164 (2.62 Å)	−7.5	ARG553 (2.65 Å), LYS621 (3.03 Å), CYS622 (2.59 Å), ASP623 (2.40 Å)

Paper

Fig. 3 2D and 3D representations of interactions of **1**, darunavir, and lopinavir with proximal amino acid residues of the SARS-CoV-2 main protease (M^pro).

Compared to **1**, the docking scores of lopinavir are similar to binding affinities of -9.8 and -7.5 kcal mol^{-1} towards M^{pro} and RdRp, respectively. In contrast, darunavir showed lower docking scores of -8.2 and -4.4 kcal mol^{-1} with M^{pro} and RdRp, respectively. Together these results provide quantitative data of the binding affinities of **1** as promising SARS-CoV-2 M^{pro} and RdRp inhibitor.

Molecular target prediction and network analysis

Using Swiss Target Prediction software, gene overlap between predicted responses activated by **1** and protein targets associated with severe acute respiratory syndrome diseases showed EGFR, MAPK14, and CTSL, as illustrated in the Venn diagram comparison (Fig. 5). Epidermal growth factor receptor (EGFR) inhibition may prevent an extreme fibrotic response to SARS-CoV and other respiratory viral infections and modulate the wound healing response to SARS-CoV.[27] MAPK14 inhibition is predicted to block the ACE2 signaling pathway, and in turn, reduce cell internalization of SARS-CoV-2.

Fig. 4 2D and 3D representations of interactions of **1**, darunavir, and lopinavir with proximal amino acid residues of the SARS-CoV-2 RNA-dependent RNA polymerase (RdRp).

Angiotensin-converting enzyme 2 (ACE2) is a host protein and the receptor for SARS-CoV-2 entry.[28] The cysteine protease cathepsin L (CTSL) is implicated in several types of pathology, and its inhibition plays a role in controlling inflammation, counterproductive immune responses. Besides, CTSL is an alternate molecular marker for drug design against SARS.[29] The development of protease inhibitors able to inhibit CTSL, CTSB, and related proteases would be an excellent starting point for the development of broad-spectrum antiviral therapies. Targets genes activated by compound **1** were also analyzed via a STRING-PPI network and visualized by Cytoscape 3.8.0. EGFR

Fig. 5 (A) Venn diagram analysis of **1** and SARS disease genes and (B) STRING PPI network for the top 10 targets identified by network analyzer for **1** as potent SARS-CoV-2 inhibitor.

and MAPK14 were observed among the top 10 scored genes for **1** (Table S1†).

Chemosystematic significance

From *F. vesceritensis* collected from the Algerian Sahara, our team and others isolated and identified several compounds mainly sesquiterpenes such as feselol, 13-hydroxyfeselol, 3-angeloxycoladonin, ferulsinaic acid, (−)-samarcandone, 1-methoxy-β-ʟ-glucopyranoside, lapiferin, 10-hydroxylancerodiol-6-anisate, 2,10-diacetyl-8-hydroxyferutriol-6-anisate, 10-hydroxylancerodiol-6-benzoate, vesceritenone and epoxy-vesceritenol, farnesiferol A, 2-acetyl-jaechkeanadiol-6-anisate, lasidiol-10-anisate, 10-oxojaesckeanadiol-6-anisate, lapidol, coladin, coladonin, lancerodiol *p*-hydroxybenzoate and jaesch-keanin.[15,16,30] In the present study, 12 secondary metabolites including two new carotene sesquiterpenes **1** and **2** were identified.

The chemotaxonomic significance of *F. vesceritensis* was established depending upon the comparison of the described chemical compounds including our isolates and the isolated compounds from other *Ferula* ecospecies around the world. Our results as well as previous studies[15,16,30] have found that isolated sesquiterpenes comprise mainly of daucane and/or carotene type sesquiterpenes in addition to some sesquiterpene couma-rins. This first overview showed complete agreement between the isolates of our plant and all described metabolites from other *Ferula* species.[14] In addition to daucane-type sesquiter-penes, sesquiterpene lactone and glycosides are commonly described sesquiterpenes from the genus such as *F. hermo-nis*,[4,25,31] *F. communis* subsp. *communis*[21], *F. varia*,[32] *F. Diversi-vittata*,[33] *F. Sinaica*,[24] and *F. jaeschkeana*.[34] A genetic correlation between *F. vesceritensis* and other *Ferula* species were deduced *via* an overlap of sesquiterpenes and sesquiterpenes esters and more specifically with the diversity of carotene type sesquiterpenes.

F. vesceritensis also exhibited a presence of sesquiterpene coumarins. Survey of the plants belonging to *Ferula* genus, sesquiterpene coumarins were found as one of the main char-acteristic metabolites for this genus such as *F. teterrima*, *F. sinkiangensis*,[8] *F. narthex*,[35] *F.* assa-foetida,[36] *F. tunetana*,[37] *F. fukanensis*,[38] *F. sinaica*,[23] *F. assa-foetida*[24] and others.[39] From these reports *F. vesceritensis* was deduced to be closely related with other *Ferula* species based on sesquiterpene type.

Eudesmanolide sesquiterpenes, their esters, and glycosides are present in some *Ferula* species. For examples, *F. sinaica*,[24] and *F. varia*[32,40,41] biosynthesize eudesmanolide sesquiterpenes. Also, *F. ferulioides* is observed to synthesize a diversity of unusual sesquiterpenes, including four resacetophenones, in addition to sesquiterpene coumarins with special skeleton alongside of the common sesquiterpenes in *Ferula* plants[42]

A final chemotaxonomical observation was that there are direct genetic relationships between the Algerian plant, *F. ves-ceritensis*, and the other *Ferula* ecospecies *via* the ability for biosynthetically building of the sesquiterpenes in general. More specific mapping of the *Ferula* species, *F. vesceritensis* was strongly correlated with all *Ferula* species *via* the ability to biosynthesize carotene and/or daucane sesquiterpenes esters and sesquiterpene coumarins. Also, *F. sinaica*, and *F. varia* were characterized by special types of sesquiterpenes, eudesmano-lides while *F. ferulioides* was characterized with respect to phe-nones sesquiterpenes and sesquiterpenes coumarins with special skeletons.

Experimental

General experimental procedures

Optical rotations were recorded on a JASCO P-2300 polarimeter (Tokyo, Japan). NMR spectra were measured on a Bruker 500 NMR spectrometer (USA)-500 spectrometer (500 MHz for ^{1}H and 125 MHz for ^{13}C, respectively). All chemical shifts (δ) are given in ppm units with reference to TMS as an internal standard, and coupling constants (J) are reported in Hz. HRMS experiments were performed on Fourier transform ion cyclotron mass spectrometer. High-performance liquid chromatography (HPLC) was performed on an Agilent pump equipped with an Agilent-G1314 variable wavelength UV detector at 254 nm and a semi-preparative reverse-phase column (Econosphere™, RP-C_{18}, 5 µm, 250 × 4.6 mm, Alltech, Deerfield, IL, USA). Silica gel 60 (230–400 mesh) was used for column chromatography. Pre-coated silica gel plates (Kieselgel 60 F$_{254}$, 0.25 mm) were used for TLC analyses. Spots were visualized by heating after spraying with 10% H_2SO_4.

Plant material

Roots of *F. vesceritensis* were collected during the flowering stage in March 2017 near Biskra, approximately 300 miles southeast of Algiers, Algeria by Prof. Dr Amar Zellagui, Depart-ment of Chemistry, Constantine University, where a voucher specimen has been deposited (AM#112).

Extraction and separation

Root of *F. vesceritensis* (1 kg) was crushed and extracted with CH_2Cl_2–MeOH (1 : 1) at room temperature. The extract was concentrated *in vacuo* to obtain a residue (30 g). The residue was fractionated by silica gel CC (6 × 120 cm) eluted with *n*-hexane (3 L), followed by a gradient of *n*-hexane–CH_2Cl_2 up to 100% CH_2Cl_2 and CH_2Cl_2–MeOH up to 15% MeOH (2 L of each solvent mixture).

The *n*-hexane : CH_2Cl_2 (1 : 1) fraction (3.5 g) was subjected to a second silica gel column (3 × 120 cm) eluted with *n*-hexane : CH_2Cl_2 (6 : 1) generating two subfractions. Subfraction 1A (0.8 g) was further purified by HPLC eluted with MeOH : H_2O (80 : 20). The flow rate was set to 1.5 mL min^{-1} and was at 0–70 min to afford **1** (10 mg, purity >98% by HPLC), (eluent hexane/EtOAc 2 : 1, R_f = 0.45) and **2** (15 mg purity >96% by HPLC), (eluent hexane/EtOAc 2 : 1, R_f = 0.40). Subfraction 2A (1 g) was also purified by HPLC eluted with MeOH : H_2O (75 : 25) The flow rate was set at 1.5 mL min^{-1} was at 0–60 min to afford **3** (25 mg, purity >98% by HPLC), (eluent hexane/EtOAc 1 : 2, R_f = 0.25), **4** (25 mg, purity >97% by HPLC), (eluent *n*-hexane/EtOAc 1 : 1, R_f = 0.45) and **10** (35 mg, purity >98% by HPLC), (eluent hexane/EtOAc 1 : 2, R_f = 0.30). An *n*-hexane CH_2Cl_2

(1 : 3) fraction (3.3 g) was subjected to a silica gel fractionation (3 × 120 cm) eluted with n-hexane–CH_2Cl_2–MeOH to give two subfractions. Subfraction 1B (1.2 g) was further purified by HPLC eluted with MeOH : H_2O (70 : 30). The flow rate was set at 2.0 mL min^{-1} was at 0–60 min to afford **5** (25 mg, purity >98% by HPLC), eluded with n-hexane/EtOAc 1 : 2, R_f = 0.25), **6** (15 mg, purity >98% by HPLC), eluded with n-hexane/EtOAc 1 : 2, R_f = 0.33), **7** (20 mg, purity >98% by HPLC, eluded with n-hexane/EtOAc 1 : 2, R_f = 0.30) and **8** (10 mg, purity >98% by HPLC), eluded with n-hexane/EtOAc 1 : 2, R_f = 0.35); subfraction 2B (1.5 g) was also purified by HPLC eluted with MeOH : H_2O (70 : 30). The flow rate was set at 1.5 mL min^{-1} was at 0–60 min to afford **9** (12 mg, purity >98% by HPLC), (eluent n-hexane/EtOAc 1 : 1, R_f = 0.40). The 100% CH_2Cl_2 fraction was subjected to HPLC eluted with MeOH : H_2O (65 : 35). The flow rate was set at 2.0 mL min^{-1} was at 0–60 min to afford **11** (17 mg, purity >96% by HPLC), (eluent n-hexane/EtOAc 1 : 2, R_f = 0.45) and **12** (17 mg, purity >97% by HPLC), (eluent n-hexane/EtOAc 1 : 2, R_f = 0.40).

8α-Anisate-dauc-4-ene-3,9-dione (webiol anisate) (1). A reddish amorphous powder; $[\alpha]_D^{25}$ +56.9 (c 0.001 MeOH); ^1H and ^{13}C NMR data, see Table 1; HRTOF-ESI-MS m/z 407.1793 [M + Na H]$^+$ (calcd for $C_{23}H_{28}NaO_5^+$, 407.1807).

10β-Acetoxy-6α-benzoate-jaeschkeanadiol (2). A reddish amorphous powder; $[\alpha]_D^{25}$ +20 (c 0.001 MeOH); ^1H and ^{13}C NMR data, see Table 1; HRTOF-ESI-MS m/z 400.2249 [M]$^+$ (calcd for $C_{24}H_{32}O_5^+$, 400.2222).

Molecular docking calculations

Autodock4.2 software was used to perform all molecular docking calculations.[43] The crystal structures of SARS-CoV-2 main protease (M^{pro}; PDB code: 6LU7 (ref. 44)) and RNA-dependent RNA polymerase (RdRp; PDB code: 6M71 (ref. 45)) were taken as templates. Water molecules, ions, and ligand, if exist, were deleted. H^{++} server was chosen to study the protonation state of M^{pro} and RdRp, and all missing hydrogen atoms were accordingly added.[46] Default docking parameters were employed, except the number of genetic algorithm (GA) run and the maximum number of energy evaluation (eval). The GA and eval values were set to 250 and 25 000 000, respectively. The docking grid was set to 60 Å × 60 Å × 60 Å with a grid spacing value of 0.375 Å. The grid center was placed at the center of the active site of M^{pro} and RdRp. Prior to molecular docking, 3D structures of the isolated compounds were minimized using SZYBKI software with MMFF94S force field software (SZYBKI, 2016). The partial atomic charges for the compounds were calculated using Gasteiger method.[47] The predicted binding poses for each compound were processed by the built-in clustering analysis (1.0 Å RMSD tolerance), and the lowest energy conformation from the largest cluster was selected as representative.

Protein–protein interactions

The online web-based tools of Swiss Target Prediction (http://www.swisstargetprediction.ch) were applied to predict the biological targets for the most promising isolated compounds as SARS-CoV-2 inhibitors. The Dis Ge NET online database (https://www.disgenet.org) was utilized to collect the available database for SARS diseases. Venn diagram was designed using Interacti-Venn online tool.[48] Protein–protein interaction (PPI) network was generated using a functional database of STRING for top predicted targets.[49] Cytoscape 3.8.0 was employed to investigate target-function relation based on the network topological.[50]

Conclusion

Ferula vesceritensis root extract afford two new sesquiterpenes, 8α-anisate-dauc-4-ene-3,9-dione (webiol anisate) (**1**) and 10α-acetoxy-6α-benzoate-jaeschkeanadiol (**2**) and ten known secondary metabolites. All compounds were *in silico* tested as anti-COVID-19 drugs using the main protease (M^{pro}) and RNA-dependent RNA polymerase (RdRp). The binding affinities indicated that **1** was a promising SARS-CoV-2 M^{pro} and RdRp inhibitor.

Conflicts of interest

The authors declare no conflict of interest.

Acknowledgements

Notes and references

1 L. Boulos, *Medicinal Plants of North Africa*, Reference Publications, Algonac, 1983, p. 183.

2 U. Yaqoob and I. A. Nawchoo, *J. King Saud Univ., Sci.*, 2017, **29**, 19–27.

3 A. H. Al-Ja'fari, R. Vila, B. Freixa, F. Tomi, J. Casanova, J. Costa and S. Canigueral, *Phytochemistry*, 2011, **72**, 1406–1413.

4 A. A. Auzi, A. I. Gray, M. M. Salem, A. A. Badwan and S. D. Sarker, *J. Asian Nat. Prod. Res.*, 2008, **10**, 711–717.

5 K. Tamemoto, Y. Takaishi, B. Chen, K. Kawazoe, H. Shibata, T. Higuti, G. Honda, M. Ito, Y. Takeda, O. K. Kodzhimatov and O. Ashurmetov, *Phytochemistry*, 2001, **58**, 763–767.

6 M. Paydar, Y. L. Wong, B. A. Moharam, E. Movahed, W. F. Wong and C. Y. S. Looi, *J. Med. Sci.*, 2013, **13**, 236.

7 P. K. Upadhyay, S. Singh and G. Agrawal, *Int. J. Green Pharm.*, 2017, **11**(2), 240–247.

8 J.-R. Yang, Z. An, Z.-H. Li, S. Jing and H.-L. Qina, *Chem. Pharm. Bull.*, 2006, **54**, 1595–1598.

9 M. Sayah and A. Mandegari, *Iran. Biomed. J.*, 2003, **7**, 139–144.

10 H. Zhang, J. Lu, L. Zhou, L. Jiang and M. Zhou, *Int. J. Clin. Exp. Med.*, 2015, **8**, 20845–20852.

11 M. Moradzadeh, H. R. Sadeghnia, S. H. Mousavi, M. Mahmoodi and A. Hosseini, *Cell. Mol. Biol.*, 2017, **63**, 17–22.

12 F. Poli, G. Appendino, G. Sacchetti, M. Ballero, N. Maggiano and F. O. Ranelletti, *Phytother. Res.*, 2005, **19**, 152–157.

13 M. Ghanbari, M. Zahedi Khorasani and A. Vakili, *Journal of Medicinal Plants*, 2012, **3**, 62–68.

14 M. Mohammadhosseini, A. Venditti, S. D. Sarker, L. Nahar and A. Akbarzadeh, *Ind. Crops Prod.*, 2019, **129**, 350–394.

15 K. Oughlissi-Dehak, P. Lawton, S. Michalet, C. Bayet, N. Darbour, M. Hadj-Mahammed, Y. A. Badjah-Hadj-Ahmed, M. G. Dijoux-Franca and D. Guilet, *Phytochemistry*, 2008, **69**, 1933–1938.

16 A. A. Ahmed, M. E. Hegazy, A. Zellagui, S. Rhouati, T. A. Mohamed, A. A. Sayed, M. A. Abdella, S. Ohta and T. Hirata, *Phytochemistry*, 2007, **68**, 680–686.

17 WHO, J World Health Organization, Geneva, available *via* https://www.who.int/dg/speeches/detail/who-director-general-s-remarks-at-the-media-briefing-on-2019-ncov-on-11-february-2020, accessed, 2020, 10.

18 M. Miski and T. J. Mabry, *Phytochemistry*, 1985, **24**, 1735–1741.

19 G. Appendino, J. Jakupovic, S. Alloatti and M. Ballero, *Phytochemistry*, 1997, **45**, 1639–1643.

20 D. Lamnaouer, M.-T. Martin, D. Molho and B. Bodo, *Phytochemistry*, 1989, **28**, 2711–2716.

21 S. Dall'Acqua, M. A. Linardi, F. Maggi, M. Nicoletti, V. Petitto, G. Innocenti, G. Basso and G. Viola, *Bioorg. Med. Chem.*, 2011, **19**, 5876–5885.

22 M. Pinar and B. Rodríguez, *Phytochemistry*, 1977, **16**, 1987–1989.

23 A. A. Ahmed, *Phytochemistry*, 1999, **50**, 109–112.

24 A. A. Ahmed, M. H. Abdel-Razek, M. I. Nassar, S. Izumi, S. Ohta and T. Hirata, *Phytochemistry*, 2001, **57**, 513–515.

25 A. Lhuillier, N. Fabre, E. Cheble, F. Oueida, S. Maurel, A. Valentin, I. Fouraste and C. Moulis, *J. Nat. Prod.*, 2005, **68**, 468–471.

26 C. Harrison, *Nat. Biotechnol.*, 2020, **38**, 379–381.

27 T. Venkataraman and M. B. Frieman, *Antiviral Res.*, 2017, **143**, 142–150.

28 M. Hoffmann, H. Kleine-Weber, S. Schroeder, N. Krüger, T. Herrler, S. Erichsen, T. S. Schiergens, G. Herrler, N.-H. Wu, A. Nitsche, M. A. Müller, C. Drosten and S. Pöhlmann, *Cell*, 2020, **181**, 271–280.

29 Y. Zhou, P. Vedantham, K. Lu, J. Agudelo, R. Carrion Jr, J. W. Nunneley, D. Barnard, S. Pöhlmann, J. H. McKerrow and A. R. Renslo, *Antiviral Res.*, 2015, **116**, 76–84.

30 A. M. Gamal-Eldeen and M. E. F. Hegazy, *Nat. Prod. Res.*, 2010, **24**, 246–257.

31 Z. Z. Ibraheim, W. M. Abdel-Mageed, H. Dai, H. Guo, L. Zhang and M. Jaspars, *Phytother. Res.*, 2012, **26**, 579–586.

32 S.-i. Kurimoto, K. Suzuki, M. Okasaka, Y. Kashiwada, O. K. Kodzhimatov and Y. Takaishi, *Phytochem. Lett.*, 2012, **5**, 729–733.

33 M. Iranshahi, A. Sahebkar, S. Hosseini, M. Takasaki, T. Konoshima and H. Tokuda, *Phytomedicine*, 2010, **17**, 269–273.

34 M. Singh, A. Agnihotri, S. Garg, S. Agarwal, D. Gupta, G. Keshri and V. Kamboj, *Planta Med.*, 1988, **54**, 492–494.

35 A. Amin, E. Tuenter, P. Cos, L. Maes, V. Exarchou, S. Apers and L. Pieters, *Molecules*, 2016, **21**, 1287.

36 M. H. Abd El-Razek, S. Ohta, A. A. Ahmed and T. Hirata, *Phytochemistry*, 2001, **58**, 1289–1295.

37 A. Jabrane, H. B. Jannet, Z. Mighri, J. F. Mirjolet, O. Duchamp, F. Harzallah-Skhiri and M. A. Lacaille-Dubois, *Chem. Biodivers.*, 2010, **7**, 392–399.

38 T. Motai and S. Kitanaka, *Chem. Pharm. Bull.*, 2004, **52**, 1215–1218.

39 Z. E. Nazari and M. Iranshahi, *Phytother. Res.*, 2011, **25**, 315–323.

40 S. Kurimoto, K. Suzuki, M. Okasaka, Y. Kashiwada, O. K. Kodzhimatov and Y. Takaishi, *Chem. Pharm. Bull.*, 2012, **60**, 913–919.

41 K. Suzuki, M. Okasaka, Y. Kashiwada, Y. Takaishi, G. Honda, M. Ito, Y. Takeda, O. K. Kodzhimatov, O. Ashurmetov and M. Sekiya, *J. Nat. Prod.*, 2007, **70**, 1915–1918.

42 T. Liu, S. Wang, L. Xu, W. Fu, S. Gibbons and Q. Mu, *Chem. Biodivers.*, 2015, **12**, 599–614.

43 G. M. Morris, R. Huey, W. Lindstrom, M. F. Sanner, R. K. Belew, D. S. Goodsell and A. J. Olson, *J. Comput. Chem.*, 2009, **30**, 2785–2791.

44 Z. Jin, X. Du, Y. Xu, Y. Deng, M. Liu, Y. Zhao, B. Zhang, X. Li, L. Zhang, C. Peng, Y. Duan, J. Yu, L. Wang, K. Yang, F. Liu, R. Jiang, X. Yang, T. You, X. Liu, X. Yang, F. Bai, H. Liu, X. Liu, L. W. Guddat, W. Xu, G. Xiao, C. Qin, Z. Shi, H. Jiang, Z. Rao and H. Yang, *bioRxiv*, 2020, DOI: 10.1101/2020.02.26.964882.

45 Y. Gao, L. Yan, Y. Huang, F. Liu, Y. Zhao, L. Cao, T. Wang, Q. Sun, Z. Ming, L. Zhang, J. Ge, L. Zheng, Y. Zhang, H. Wang, Y. Zhu, C. Zhu, T. Hu, T. Hua, B. Zhang, X. Yang, J. Li, H. Yang, Z. Liu, W. Xu, L. W. Guddat, Q. Wang, Z. Lou and Z. Rao, *Science*, 2020, **368**, 779–782.

46 J. C. Gordon, J. B. Myers, T. Folta, V. Shoja, L. S. Heath and A. Onufriev, *Nucleic Acids Res.*, 2005, **33**, W368–W371.

47 J. Gasteiger and M. Marsili, *Tetrahedron*, 1980, **36**, 3219–3228.

48 H. Heberle, G. V. Meirelles, F. R. da Silva, G. P. Telles and R. Minghim, *BMC Bioinf.*, 2015, **16**, 169.

49 R. Li, X. Ma, Y. Song, Y. Zhang, W. Xiong, L. Li and L. Zhou, *J. Cell. Biochem.*, 2019, **120**, 11265–11273.

50 P. Shannon, A. Markiel, O. Ozier, N. S. Baliga, J. T. Wang, D. Ramage, N. Amin, B. Schwikowski and T. Ideker, *Genome Res.*, 2003, **13**, 2498–2504.